

# Diffraction-limited bispectrum speckle interferometry of the Herbig Be star R Mon<sup>\*</sup>

G. Weigelt<sup>1</sup>, Y. Y. Balega<sup>2</sup>, K.-H. Hofmann<sup>1</sup>, and T. Preibisch<sup>1</sup>

<sup>1</sup> Max-Planck-Institut für Radioastronomie, Auf dem Hügel 69, 53121 Bonn, Germany

<sup>2</sup> Special Astrophysical Observatory, Nizhnij Arkhyz, Zelenchuk region, Karachai-Cherkesia 357147, Russia

Received 17 May 2002 / Accepted 21 June 2002

**Abstract.** We explore the structures immediately surrounding the intermediate-mass young stellar object R Mon with bispectrum speckle interferometry, conventional near-infrared imaging and by analyzing optical HST archive data. Our near-infrared speckle images with unprecedented diffraction-limited resolution of 55 mas ( $\sim 44$  AU;  $H$ -band) and 76 mas ( $\sim 61$  AU;  $K$ -band) represent the highest resolution R Mon images obtained so far and exhibit previously unseen complex structures. While the binary companion R Mon B appears as an unresolved point source in our speckle images, the image of the primary R Mon A is marginally extended in the  $K$ -band and significantly extended in the  $H$ -band. The most prominent new feature is a bright arc-shaped structure, pointing away from R Mon in north-western direction. We interpret this feature as the surface of a dense structure near the thick circumstellar disk or torus around R Mon. Our images also reveal several twisted filaments of helical shape which are similar to the twisted filaments in the outer parts of the nebula. We identify structures which probably are responsible for casting pronounced shadows in the outer regions of the NGC 2261 reflection nebula. Finally, we discuss the relation of the observed features, in particular the arc-shaped speckle feature, to the wind and outflow activity (Herbig-Haro objects and jets) of R Mon.

**Key words.** techniques: interferometric – stars: individual: R Mon – stars: formation – stars: winds, outflows

## 1. Introduction

The variable star R Mon belongs to the group of Herbig Ae/Be stars (see Herbig 1960; Finkenzeller & Mundt 1984; Thé et al. 1994), i.e. it is an intermediate-mass pre-main sequence star. R Mon is located at a distance of about 800 pc (Jones & Herbig 1982) and illuminates the famous fan-shaped reflection nebula NGC 2261, also known as Hubble's variable nebula. This nebula displays strong variability on timescales of months (e.g. Lightfoot 1989). A summary of observational results on R Mon and NGC 2261 can be found in the review by Staude & Elsässer (1993). CO radio observations showed that R Mon is located in a massive extended flattened molecular torus and drives a bipolar outflow in north-south direction (Canto et al. 1981). Jones & Herbig (1982) detected a small group of Herbig-Haro objects, HH 39, about  $7.5'$  north of R Mon at a position angle of  $350^\circ$ , i.e. on the symmetry axis of the NGC 2261 nebula. Brugel et al. (1984) discovered

highly collimated bipolar outflows about  $10''$  north and south of R Mon, providing evidence for ongoing high-velocity outflow activity from R Mon. While the northern part of the optical reflection nebula is very prominent, only very faint nebulosity is seen in the south of R Mon (Walsh & Malin 1985). This suggests that the outflow axis is tilted against the plane of the sky, with the (blue-shifted) northern lobe pointing towards the observer, while the (red-shifted) southern lobe is tilted away from the observer and presumably obscured by dusty material in a flattened circumstellar structure.

Herbig (1968) was the first to notice that R Mon is not a point source in optical images but has the shape of a triangular nebula. He concluded that the visible light does not come directly from the star but from a small nebula. The shape and orientation of this nebula continues out into the much larger fan of NGC 2261. These results suggest that the star is surrounded by a thick circumstellar disk or a torus, in which a conical cavity was carved out by the outflowing material. The nebular emission is thought to be mainly reflected light from the bright inner wall of this cavity. Lightfoot (1989) performed detailed modeling of the structures in the reflection nebula based on the cavity model.

Aspin et al. (1988) presented the first detailed near-infrared images of R Mon and NGC 2261. The first near-infrared speckle interferometric observations of R Mon were presented

Send offprint requests to: G. Weigelt,  
e-mail: weigelt@mpifr-bonn.mpg.de

\* Part of the results presented in this paper are based on observations obtained at the German-Spanish Astronomical Centre, Calar Alto, operated by the Max-Planck-Institute for Astronomy, Heidelberg, jointly with the Spanish National Commission for Astronomy. The speckle data were collected at the Special Astrophysical Observatory with the 6 m telescope.

by Beckwith et al. (1984) and suggested a halo with a size of  $1300 \times 1300$  AU around the central object. Further speckle observations of R Mon by Leinert et al. (2001) resolved the halo into two components with sizes of  $0.4''$  and  $3''$ .

A comprehensive study of R Mon, including high-resolution near-infrared adaptive optics imaging and polarimetry, mid-infrared imaging, analysis of HST images, and theoretical modeling, was presented by Close et al. (1997; C97 hereafter). In this study, a binary companion with a separation of  $0.69''$  from R Mon was discovered. The direct extinction towards the central star was determined to be  $A_V = 13$  mag. C97 modeled the system as a young stellar object surrounded by an optically and geometrically thick accretion disk that is embedded in an extended dusty envelope. According to this model, the jet from R Mon (which has an inclination angle of  $20^\circ$  relative to the plane of the sky) has cleared a conical cavity in the envelope, through which light escapes and illuminates the NGC 2261 reflection nebula (see Fig. 15 in C97 for a cartoon illustrating the geometry of the dust distribution). The images presented by C97 also revealed a complex of twisted filaments with a double-helical structure along the eastern edge of the parabolic shell, which may trace a twisted magnetic field above R Mon.

## 2. Observations and data reduction

The speckle interferograms were recorded with the 6 m SAO telescope on 26 and 27 September 1999. The detector of our speckle camera was a Rockwell HAWAII array detector. The observations were made through  $K$ -band and  $H$ -band filters with center wavelength/ $FWHM$  bandwidth of  $2.15 \mu\text{m}/0.21 \mu\text{m}$  and  $1.65 \mu\text{m}/0.32 \mu\text{m}$ . The pixel sizes of the  $K$ -band and  $H$ -band observations were  $26.4$  mas and  $20.1$  mas, respectively. The exposure time per frame was  $160$  ms. The  $K$ -band data set consists of 1175 R Mon speckle interferograms and 1024 speckle interferograms of the unresolved reference star HIP 30939. The  $H$ -band data set consist of 815 R Mon speckle interferograms and 607 speckle interferograms of HIP 30939. The total integration times of the R Mon datasets are  $188$  s ( $K$ -band) and  $130$  s ( $H$ -band), the integration times of the reference star datasets are  $164$  s ( $K$ -band) and  $97$  s ( $H$ -band). The field-of-view was  $5.0'' \times 5.0''$  for the  $K$ -band observation, and  $5.1'' \times 5.1''$  for the  $H$ -band observation. The seeing ( $FWHM$ ) was  $\sim 0.8''$ .

Diffraction-limited images were reconstructed using the bispectrum speckle interferometry method (Weigelt 1977; Lohmann et al. 1983; Hofmann & Weigelt 1986). The object power spectrum was determined with the speckle interferometry method (Labeyrie 1970). Speckle interferograms of unresolved single stars were recorded just before and after the object and served as reference stars for the determination of the speckle transfer function. The resulting  $K$ - and  $H$ -band images are diffraction-limited with a resolution of  $76$  mas and  $56$  mas, respectively. The faintest nebula structures visible in our speckle images are approximately 500 times fainter than the peak brightness (see Fig. 4).

We also investigated archival HST WFPC2 images of R Mon: a 300 s  $V$ -band image, a 300 s  $I$ -band image, and 300 s

and 6 s  $R$ -band images. In all these images R Mon is located on the PC chip. At the PC pixel scale of  $45.5$  mas per pixel, the images are under-sampled and have an effective resolution of  $\sim 100$  mas. As the central part of the long-exposure HST images is saturated, we created an unsaturated  $R$ -band image by replacing the saturated pixels in the long-exposure  $R$ -band image by the scaled pixel values from the un-saturated short-exposure  $R$ -band image.

Near infrared seeing-limited images of R Mon were obtained in October 2000 with the Omega Prime wide-field near-IR camera (Bizenberger et al. 1998) on the Calar Alto 3.5 m telescope. The camera uses a  $1024 \times 1024$  pixel HgCdTe array with  $0.4''$  per pixel. Images were taken through a standard  $J$ -band filter, a non-standard  $H_s$  filter ( $1.49$ – $1.64 \mu\text{m}$ ), and a broad-band  $K'$  filter ( $1.94$ – $2.29 \mu\text{m}$ ). We also took images through the 1% filter NB2122, centered on the  $v = 1-0$  S(1) line of the  $\text{H}_2$  molecule at  $2.12 \mu\text{m}$ . In each of these filters, images were taken at 6 different dither positions with positional shifts of  $40''$ ; at each position a series of 10 images with exposure times of 3 s ( $J$ -band and  $H_s$  band), 20 s (NB2122), and 1.7 s ( $K'$ -band) was taken. The weather conditions during our observations were good, the seeing (as measured by the  $FWHM$  of the PSF in our images) was  $\sim 1.2''$ – $1.6''$ . Standard data reduction techniques were used to sky subtract, flat field, and mosaic the data (cf. McCaughrean et al. 1994). The field-of-view of the final images is  $7.8' \times 7.8'$ .

To search for  $\text{H}_2$  emission, we carefully aligned the NB2122 filter image with the  $K'$  filter image via several point sources in the outer regions of the image and subtracted the  $K'$  filter image from the NB2122 filter image. The resulting continuum subtracted  $\text{H}_2$  emission line image did not reveal any features exceeding the noise level. This is consistent with the non-detection of molecular hydrogen emission in the infrared spectrum of R Mon (Kelly et al. 1994). Note that the field-of-view of our  $\text{H}_2$  image does *not* include the Herbig-Haro object HH 39, which is  $7.5'$  north of R Mon.

## 3. Interpretation of the observed structures

In Fig. 1 we present our diffraction-limited speckle images, optical images derived from HST WFPC archive data, and our seeing-limited near-infrared images of R Mon. Figure 2 shows the full field of our  $H$ -band speckle image with annotations of all the features discussed in the text below. The first thing to note when comparing our near-infrared speckle images with the optical HST image (Fig. 1c) is the different morphology of the diffuse structures. This can be understood as the consequence of the optical depth to the central source: as determined by C97, the extinction along the line-of-sight towards R Mon is  $A_V = 13$  mag. This means that the circumstellar material around R Mon is optically thick in the optical bands, e.g.  $\tau_R = 9.7$ ; we see no direct light from the central object but only light scattered at the nebulous circumstellar structures. In the near infrared, however, the optical depth is only  $\tau_H = 2.2$  and  $\tau_K = 1.4$ ; therefore these images are dominated by direct light from the central source and emission from hot circumstellar material. We now discuss the various features seen around R Mon.

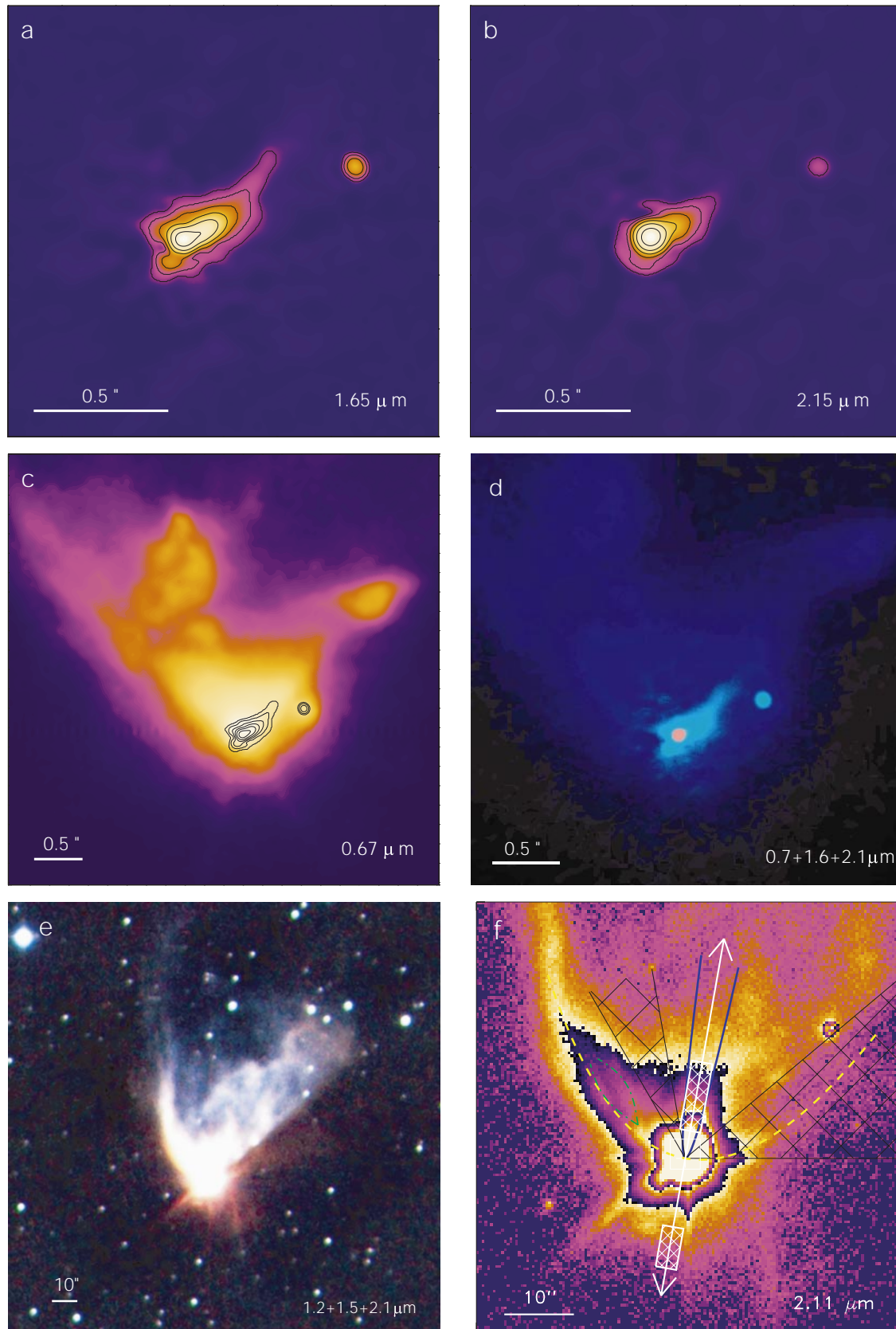


**Fig. 1.** **a,b)** Central parts of our *H*- and *K*-band speckle images of R Mon. **c)** HST *R*-band image with contours of the *H*-band speckle image. **d)** True-color composite of the *R*-band (blue) HST image and the *H*- (turquoise) and *K*-band (red) speckle images (the colors are discussed in Sect. 3.3). **e)**  $JH_sK'$  color composite image derived from the Calar-Alto data. **f)** Calar-Alto *K'*-band image (wrapped intensity scale) of the inner nebula with annotations (for explanations see Sects. 3.5 and 3.6).

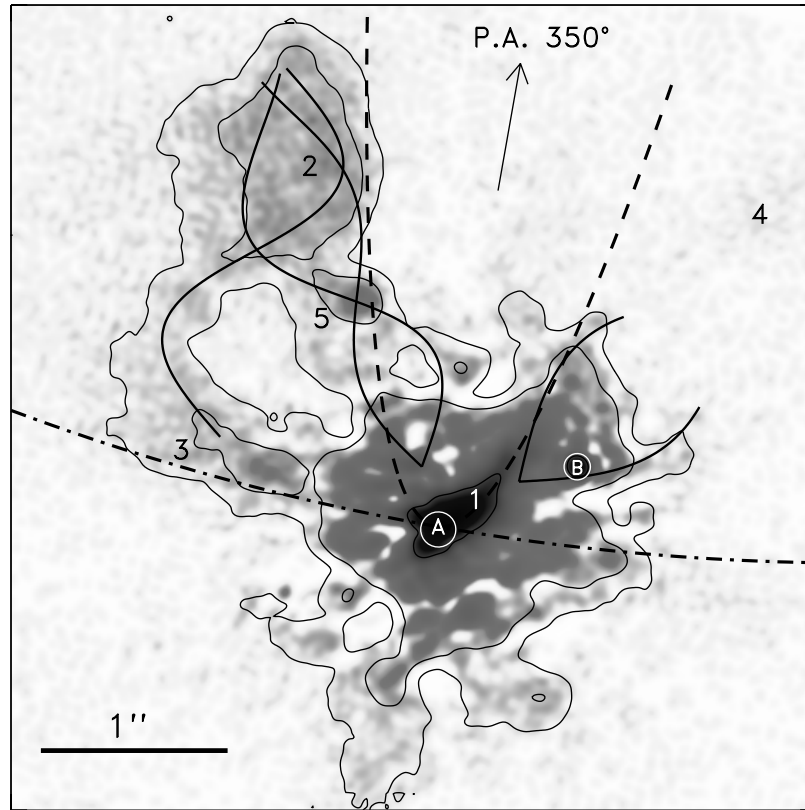


**Fig. 2.** Greyscale + contour representation of our *H*-band speckle image with annotation of the features discussed in the text. The intensity scale is based on a power-law relation and was adjusted to show both the central bright as well as the outer faint structures with good contrast. The locations of R Mon A and R Mon B are marked by white circles. The features 1–5 are marked. The dashed line shows the inner parabola defined in the text. The dashed-dotted line shows the parabola defined by the large-scale structure of the nebula (yellow line in Fig. 1f). The solid sin-curves mark the helical features.

### 3.1. R Mon A and R Mon B

R Mon B is an unresolved point source in both the diffraction-limited *H*-band speckle image (resolution 55 mas) and the diffraction-limited *K*-band image (resolution 76 mas). In contrast to the optical images, in which R Mon A is a small triangular-shaped nebula, our *K*-band speckle image shows R Mon A to be a nearly point-like source; we find a *FWHM* Gaussian diameter of 83 mas in east-west direction and 78 mas in north-south direction (i.e., the R Mon image is only a few mas larger than the 76 mas Airy disk). In our *H*-band image, R Mon A has a *FWHM* Gaussian diameter of 153 mas in east-west direction and 81 mas in north-south direction, i.e. is clearly more extended.

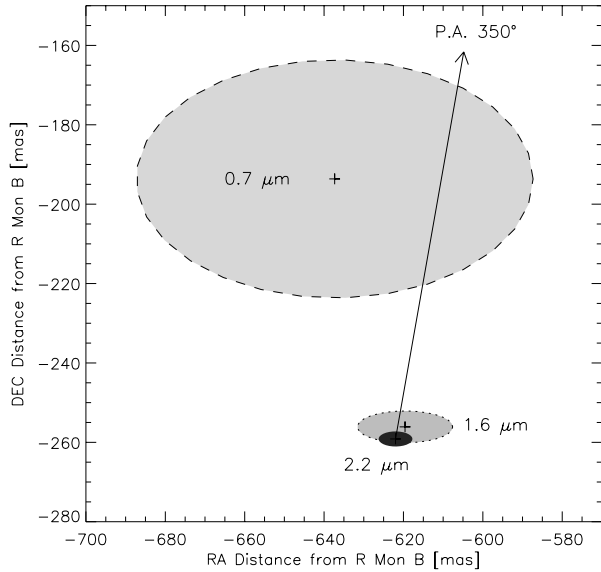
Our images also allow a very precise determination of the wavelength-dependent position of the brightness peak (R Mon A) relative to R Mon B. In our *H*-band image we find an angular separation of  $670 \pm 8$  mas and  $\text{PA } 292.5^\circ \pm 0.4^\circ$ , in our *K*-band image we find  $674 \pm 3$  mas and  $\text{PA } 292.6^\circ \pm 0.2^\circ$ . From the HST *R*-band image we determine a separation of  $666 \pm 30$  mas and  $\text{PA } 287^\circ \pm 1^\circ$ .

Figure 3 shows the positional offsets of the central brightness peak (R Mon A) from R Mon B at the different wavelengths. One can see that the central brightness peak moves *northward* with decreasing wavelength; the direction of the shift has a similar orientation as the symmetry axis of the

large-scale nebula (PA  $350^\circ$ ). While the positional shift between the *H*-band and the *K*-band peak is very small and barely significant, the *R*-band peak is shifted by  $\sim 65$  mas relative to the *K*-band peak. The shift of R Mon A's position from infrared to optical wavelengths was already noted by C97 and can be understood as the consequence of the extinction along the line-of-sight towards R Mon: in the infrared *K*-band we directly see R Mon A or light from its innermost ( $\lesssim 2$  AU) circumstellar environment, whereas in the optical *R*-band the star is hidden and we see only scattered light from outer regions ( $\gtrsim 50$  AU) of the circumstellar environment.

### 3.2. General structure of the diffuse features within $2''$ from R Mon

In contrast to the relatively symmetric appearance of the optical nebula around R Mon in the HST image, our near-infrared speckle images (Figs. 1a,b and 2) show a very pronounced asymmetry. The most prominent structure in our speckle images (Figs. 1a,b) is the bright arc-shaped feature extending directly from R Mon to the north-west, marked as feature 1 in Fig. 2. This structure can neither be seen in the HST data nor in the adaptive optics images (C97). Up to a distance of  $\sim 0.4''$  from R Mon, the arc is rather bright and has a well defined and sharp outline. Further out, it seems to dissolve into more



**Fig. 3.** Positional offsets between the point source R Mon B and the central brightness peak (R Mon A) at different wavelengths. The size of the filled ellipses indicates the ( $2\sigma$ ) positional uncertainties in the different wavelength bands. The arrow marks PA  $350^\circ$ , the main symmetry axis of the large-scale nebula.

extended nebulosity. The general shape of the brighter parts of this arc can approximately be described by a one-sided parabola. The arc probably represents the surface of dense material near the disk or the outer region of a torus-like structure. It points towards a region of diffuse emission right at the edge of our speckle image (feature 4), that can better be seen in the HST image.

The eastern part of our speckle image in Fig. 2 is dominated by an extended patch of diffuse emission (feature 2)  $\sim 1''$  north-east of R Mon and several faint filamentary structures. The detailed structures of the faint filaments will be discussed in Sect. 3.4.

If we fit a parabola (dashed line in Fig. 2) with symmetry axis along PA  $350^\circ$  (i.e. the direction of the outflow) to the north-western arc (feature 1), the eastern part of this parabola coincides approximately with the western boundary of feature 2. This parabola is much narrower than the large-scale parabolic shape of the extended nebula seen in conventional images (dashed-dotted line in Fig. 2 and yellow line in Fig. 1f). We interpret these two parabolic structures in the following way. The wider parabola probably represents the upper edge of a flattened circumstellar structure, presumably a thick disk or a torus, around R Mon. The space above this disk is partially filled with diffuse material, which is predominantly located close to the surface of the disk and below the narrow parabola. The space inside this narrow parabola seems to contain much less dense material or is essentially empty.

### 3.3. Colors of the diffuse features

In Fig. 1e we present a true color composite image created by combining the HST *R*-band image (blue), our *H*-band speckle image (turquoise) and our *K*-band speckle image (red).

The extended nebula, which represents scattered light, appears blue, while the central star R Mon A, which is not directly visible in the optical image, appears very red.

For a more quantitative color analysis, we have performed aperture photometry for selected features in our speckle *H*-band and *K*-band images. The measured colors were calibrated by the point source R Mon B, for which C97 determined  $H - K' = 1.9$ . We used circular apertures with radii of 72 mas for R Mon A and R Mon B. For R Mon A we find  $H - K' = 3.2$ , which is significantly redder than the color determined by C97 ( $H - K' = 1.75$ ) with PSF fitting photometry. The errors of the colors reported in this section are approximately  $\pm 0.3$  mag. When using larger apertures, the color gets bluer, e.g.  $H - K' = 2.7$  for a 400 mas aperture. The effect can be explained as an increasing contribution of (relatively bluer) scattered light with increasing aperture size.

We also placed a sequence of three apertures with radii of 72 mas along the bright arc (feature 1), centered at distances of 140 mas, 290 mas, and 430 mas from R Mon A, respectively. The resulting  $H - K'$  colors in these three regions are 2.3, 2.0, and 1.6; this demonstrates a strong color gradient along feature 1. This color gradient is well consistent with the idea that the parabolic feature represents mostly scattered light with a relatively small contribution of emission from hot circumstellar material near the center.

For the nebulous blob 2 we find  $H - K' = 1.6$  in a circular aperture with radius 416 mas. For feature 3 we find  $H - K' = 1.6$  in a circular aperture with radius 336 mas. For feature 5 we find  $H - K' = 1.7$  in a circular aperture with radius 88 mas. We also investigated intensity cuts in different directions through our images. Figure 4 shows cuts along the lines connecting R Mon A to R Mon B and to patch 2.

### 3.4. Structure of the filaments

The presence of several large twisted filamentary structures in the NGC 2261 nebula has been known for many years (see Lightfoot 1989). Some of the observed patterns can be explained as shadows from twisted helical structures near the star. The adaptive optics images of C97 revealed a twisted double helix about  $1''$  north-east of R Mon, which is associated with feature 2. While our speckle images are not as deep as the adaptive optics images of C97, they are sharper and therefore allow us to follow these filaments closer towards R Mon. Our data suggest that the innermost detectable knot of this double helix is located at a position  $\sim 0.4''$  north-east of R Mon. The shapes of the filaments can be well reproduced by sin curves running to the north-east along PA  $20^\circ$ . The spatial period of the curves is  $2.0'' \cong 1600$  AU, their width is  $\sim 0.3'' \cong 230$  AU. Our speckle image shows several additional structures that might represent similar twisted filaments. One such feature seems to connect the feature 3 with the diffuse patch 2 and is marked in Fig. 2. In the western part of our image we also find diffuse nebulosity that suggests the presence of a double helix running in north-western direction (PA  $310^\circ$ ) towards patch 4.

What is the physical nature of these filamentary structures? It has been suggested that the filaments might represent

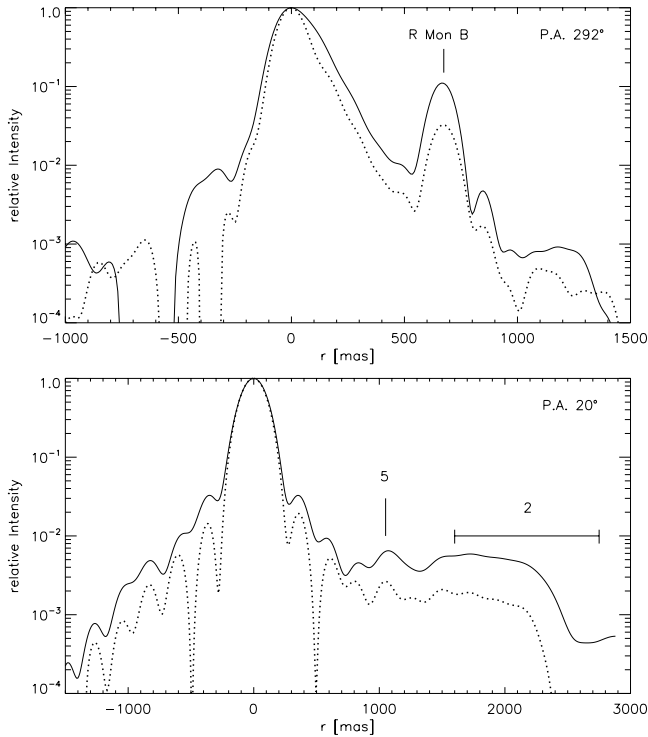


**Fig. 4.** Intensity cuts through our speckle images along two different directions. The *H*-band intensity is shown as the solid line, the *K*-band intensity as the dotted line; both curves are normalized with respect to the central peak. The direction of the cut line in the upper plot is from the central peak (at  $r = 0$ ) through R Mon B, corresponding to PA  $292^\circ$ . The cut line in the lower plot runs from the central peak through the center of feature 5 and further on through feature 2, along PA  $20^\circ$ .

partially ionized gas that is influenced by and flowing along twisted magnetic field lines (see C97). Their possible relation to the molecular outflow will be discussed in Sect. 3.6.

### 3.5. Connection between the small-scale and large-scale structure

How are the structures in the immediate vicinity of R Mon related to the large-scale structure in the NGC 2261 nebula? Figure 1e shows the large-scale morphology of the NGC 2261 nebula in a true-color composite image created from our *J*-, *H<sub>s</sub>*-, and *K'*-band wide field images obtained at the 3.5 m Calar Alto telescope. The *J*-band (blue) is dominated by scattered light in the northern lobe of the reflection nebula, whereas the obscured southern counterlobe is bright in the *K'*-band (red) only. Figure 1f shows the central part of our *K'*-band image. The main large-scale morphological features of the nebula seen in these images are as follows.

The north-eastern part of the nebula has a well defined sharp parabolic shape, as indicated by the yellow dashed line. This part of the nebula contains several twisted filaments, two of which are marked in Fig. 1f by the green dashed-dotted lines.

The north-western part of the nebula displays a quite different morphology: here, the edge of the parabolic shell is very faint and can be well seen only in the *K*-band. The diffuse

emission in the north-western part of the nebula is very extended and terminates sharply at a straight edge running along PA  $310^\circ$ . The sharpness of this edge (see Fig. 1e) suggests it to be caused by a shadow effect. The diffuse emission inside the parabolic shell predominantly seems to consist of several curved filaments.

The southern counterpart of the parabolic nebula is much fainter and can be well seen only in the *K*-band image. The south-eastern edge is dominated by a short and sharp spike along PA  $135^\circ$ . The south-western edge is traced by a curved spike pointing southwards.

Many of the morphological features of the NGC 2261 reflection nebula can be explained by shadows cast by circumstellar material close to R Mon (cf. Lightfoot 1989). It is interesting to note that the orientation of the sharp western edge in the northern diffuse emission corresponds to the direction of the bright western arc (feature 1 revealed by our speckle image). The dense material related to feature 1 can probably prevent light from R Mon to reach regions at PA less than  $310^\circ$ , and this can explain the observed large-scale shadow effect. The expected shadow region is marked by the black hatched area in Fig. 1f. The material associated with the nebulous blob 2 also might cast some shadow on the outer nebula: feature 2 covers a range of position angles of  $10^\circ$ – $30^\circ$  as seen from R Mon, and in these directions a minimum in the brightness of the extended nebulosity on the scale of  $\sim 10''$  can be seen.

### 3.6. Relation of the observed features to the outflow activity of R Mon

R Mon is the source of a stellar wind, a bipolar jet, and a bipolar molecular outflow. Jones & Herbig (1982) studied the wind of R Mon and identified two different components: a fast wind with latitude dependent velocity, flowing outwards at about  $300 \text{ km s}^{-1}$  along the polar axis (PA  $350^\circ$ ) of the system, but at only  $\sim 50 \text{ km s}^{-1}$  perpendicular to the jet axis, and another, much slower, wind component that expels circumstellar dust northward along the hollow cone of the NGC 2261 nebula at a velocity of about  $30 \text{ km s}^{-1}$ .

The first evidence for a jet from R Mon was the detection of the HH 39 group of Herbig-Haro objects, located about  $7.5'$  north of R Mon at PA  $350^\circ$  (Jones & Herbig 1982). HH 39 is moving away from R Mon at a tangential velocity of about  $290 \text{ km s}^{-1}$ , suggesting a dynamical age of  $\sim 5900$  yrs. The spatial distribution of the individual bright knots of HH 39 corresponds to a jet opening-angle of only  $\sim 2^\circ$ . Brugel et al. (1984) reported the spectroscopic detection of a bipolar jet close to R Mon, also along PA  $350^\circ$ . The northern component extends  $4''$ – $14''$  from R Mon and has a width of  $\lesssim 3''$ ; the southern component is  $10''$ – $16''$  from R Mon.

The molecular outflow from R Mon was detected in CO observations (cf. Canto et al. 1981). In contrast to the well collimated jet, the molecular outflow is very extended and poorly collimated. The northern, blue-shifted CO outflow lobe peaks  $\sim 1.5'$  from R Mon and has an opening angle of  $\sim 45^\circ$ . The southern lobe peaks  $\sim 30''$  from R Mon and is even more extended, suggesting an opening angle of  $\gtrsim 90^\circ$ .

The radial velocities of the northern and southern outflow lobes of  $\sim\pm 2 \text{ km s}^{-1}$  correspond to space velocities of  $\sim\pm 6 \text{ km s}^{-1}$ . To summarize these results, the outflow activity of R Mon consists of two main components, a fast, strongly collimated jet, and slow, poorly collimated outflow. How are these components related to the observed structures in the immediate vicinity of R Mon?

In Fig. 1 if we have marked the two jet components detected by Brugel et al. (1984) as white hatched boxes. It is interesting to note that the northern jet component fits very well into the extrapolated shape of the inner parabola defined in Fig. 2. This suggests that the mostly empty region in the interior of this inner parabola represents the path of the jet, which has cleared its way. This interpretation is supported by our non-detection of  $\text{H}_2$  emission, suggesting that there are currently no strong molecular shocks along the jet path.

The low-velocity, wide-angle outflow may be related to the numerous filaments visible in the diffuse material around R Mon and in the NGC 2261 nebula. It has been suggested (see C97) that these filaments might represent partially ionized gas that is influenced by and flowing along twisted magnetic field lines. As noted by C97, the width and the spatial period of the filaments increase strongly with increasing distance from R Mon. The twist of the field lines may have originated during the collapse of the rotating cloud core out of which R Mon formed, and now the strongly twisted field lines are unwinding. The magnetic forces applied by the unwinding field lines may well be able to drive the low-velocity outflow (cf. Uchida & Shibata 1985). If this hypothesis is correct, the filaments between the inner and the outer parabola in Fig. 1 represent the origin of the molecular outflow.

#### 4. Summary and conclusions

The main results of our high-resolution near-infrared imaging study of R Mon can be summarized as follows:

R Mon A is seen as a very red ( $H - K' = 3.2$ ) source, which is marginally extended in the  $K$ -band ( $\sim 83 \times 78 \text{ mas}$ ) and significantly extended in the  $H$ -band ( $\sim 81 \times 153 \text{ mas}$ ). Its binary companion R Mon B appears as an unresolved point source in our speckle images. We find a strong asymmetry in the immediate environment of R Mon. To the west of R Mon A, a dominant arc-shaped feature (1) provides evidence for a dense structure near the surface of the disk or torus around R Mon A. This feature shows a strong color gradient: the  $H - K'$  color changes from 2.3 mag near R Mon A to 1.6 mag at a distance of 430 mas from R Mon A, suggesting that the arc represents mostly scattered light. This arc structure is located in the region of the bipolar jet discovered by Brugel et al. (1984) and might be responsible for the observed shadow in the western part of the NGC 2261 nebula. The region to the east of R Mon A is dominated by less dense, more diffuse material, and contains several twisted filaments, which might trace magnetic field lines.

The morphological structures in the inner circumstellar environment around R Mon seem to reflect the jet- and outflow-activity of this young stellar object: the region along the polar axis of the star/disk system and inside the narrow parabola through the arc-shaped speckle feature (1) seems to be mostly free of diffuse material; probably, the fast jet from R Mon A has cleared a narrow path (outflow cavity) along the jet axis, which therefore is now mostly empty. The diffuse filamentary structures above the disk plane might trace material aligned along magnetic field lines; the unwinding of the twisted magnetic field lines may be responsible for driving the wide-angle molecular outflow from R Mon, that originates from the inner parts of the circumstellar disk around R Mon A.

*Acknowledgements.* We are grateful to the referee, L. Close, for his useful comments which helped to improve this paper. We also thank Alexander Menshchikov for useful discussions.

#### References

- Beckwith, S., Zuckerman, B., Skrutskie, M., & Dyck, H. M. 1984, *ApJ*, 287, 793
- Bizenberger, P., McCaughrean, M. J., Birk, C., Thompson, D., & Storz, C. 1998, *Proc. SPIE*, 3354, 825
- Brugel, E. W., Mundt, R., & Bührke, T. 1984, *ApJ*, 287, L73
- Canto, J., Rodriguez, L. F., Barral, J. F., & Carral, P. 1981, *ApJ*, 244, 102
- Close, L. M., Roddier, F., Hora, J. L., et al. 1997, *ApJ*, 489, 210
- Finkenzeller, K., & Mundt, R. 1984, *A&AS*, 55, 109
- Herbig, G. H. 1960, *ApJS*, 4, 337
- Herbig, G. H. 1968, *ApJ*, 152, 439
- Hofmann, K.-H., & Weigelt, G. 1986, *A&A*, 167, L15
- Hodapp, K.-W. 1990, *ApJ*, 352, 184
- Hodapp, K.-W. 1994, *ApJS*, 94, 615
- Jones, B. F., & Herbig, G. H. 1982, *AJ*, 87, 1223
- Kelly, D. M., Rieke, G. H., & Campbell, B. 1994, *ApJ*, 425, 231
- Labeyrie, A. 1970, *A&A*, 6, 85
- Leinert, Ch., Haas, M., Abraham, P., & Richichi, A. 2001, *A&A*, 375, 927
- Lightfoot, J. F. 1989, *MNRAS*, 239, 665
- Lohmann, A. W., Weigelt, G., & Wirtitzer, B. 1983, *Appl. Opt.*, 22, 4028
- McCaughrean, M. J., Zinnecker, H., & Rayner, J. T. 1994, *ApJ*, 436, L189
- Minchin, N. R., Hough, J. H., McCall, A., et al. 1991, *MNRAS*, 249, 707
- Staude, H. J., & Elsässer, H. 1993, *A&AR*, 5, 165
- Thé, P. S., de Winter, D., & Pérez, M. R. 1994, *A&AS*, 104, 315
- Uchida, Y., & Shibata, K. 1985, *PASJ*, 37, 515
- Warren-Smith, R. F., Draper, P. W., & Scarrott, S. M. 1987, *ApJ*, 315, 500
- Weigelt, G. 1977, *Opt. Commun.*, 21, 55
- Weigelt, G. 1991, in *Progress in Optics*, vol. 29, ed. E. Wolf (Elsevier Science Publishers), 295